Assignment of Resonances in the Downfield Proton Spectrum of *Escherichia coli* 5S RNA and Its Nucleoprotein Complexes Using Components of a Ribonuclease-Resistant Fragment†

Matthew J. Kime, Daniel T. Gewirth, and Peter B. Moore*

ABSTRACT: The downfield (9–15 ppm) proton NMR spectra of oligonucleotides derived from the ribonuclease A resistant fragment of *Escherichia coli* 5S RNA have been examined in aqueous solution at 500 MHz. Comparison of these spectra with those of the 5S RNA fragment and intact 5S RNA using both chemical shift and nuclear Overhauser enhancement effect criteria indicates that several aspects of 5S RNA secondary structure are also present in the structures assumed in solution by these much smaller molecules. Analysis of these spectra permits the assignment of some imino proton resonances which could not be assigned with certainty on the basis of NMR data previously obtained on intact 5S RNA or its nucleoprotein complexes. Several previous resonance assignments are confirmed. Studies on oligonucleotide components of fragment and a reconstituted fragment show that at least two conformations of the procaryotic loop exist.

The downfield proton NMR[1] spectrum (9–15 ppm) of a nucleic acid in ^1H_2O solution is dominated by base pair imino proton resonances and so is a potential source of secondary and tertiary structural information. The corresponding region of nucleoprotein complex spectra may also contain quaternary structural information as well. The ability of NMR spectroscopy to provide information about molecular structure and dynamics cannot be fully exploited, however, unless individual resonances are assigned.

The early efforts to assign downfield resonances in tRNA NMR spectra used ring current shift prediction to obtain the chemical shifts of imino protons involved in Watson–Crick base pairs in RNA helices (Shulman et al., 1973). Another, in many respects parallel, tRNA spectral assignment strategy involved the dissection of the macromolecule into fragments and comparison of the spectra of the fragments with the spectra of the parent molecules (e.g., Lightfoot et al., 1973; Reid et al., 1979; Hurd & Reid, 1979). The dissection method had only limited success [e.g., see Johnston & Redfield (1981) and Heerschap et al. (1983) for comments on some assignments made by fragment studies]. Except for a successful study of tRNA folding (Boyle et al., 1980), it appears to have been discontinued by workers in the tRNA field. More recently nuclear Overhauser enhancement (NOE) effects have been employed to assign resonances in ribonucleic acid spectra [see Roy & Redfield (1983), Hare & Reid (1982), Heerschap et al., (1983), and Kime & Moore (1983a) and references contained in these papers] and in a ribonucleoprotein complex (Kime & Moore, 1983b). In the work described here we employ a combination of all three strategies (ring current shift prediction, fragmentation, and NOEs) to extend the assignment of resonances in the *Escherichia coli* 5S RNA spectrum (Kime & Moore, 1983a,b).

Limited ribonuclease A digestion of *E. coli* ribosomal 5S RNA generates a molecule which is a trimolecular complex of three RNA strands consisting of bases 1–11, 69–87, and 89–120 of the parent molecule (Douthwaite et al., 1979). Also present in such preparations is an appreciable amount of a bimolecular complex composed of bases 1–11 and 69–120. Below we report the large scale isolation of all four of the main oligonucleotide components from 5S RNA fragment preparations, their characterization, and their NMR spectra both alone and in combination.

Assignment of the 5S RNA terminal stem helix imino proton resonances by NOE connectivity techniques is difficult because both strands in the stem (bases 1–10 and 110–120) have the sequence $^{5'}$UGCC(A or U)GGC(purine)$^{3'}$. The stem produces a set of NOE connectivities which are readily interpreted as $(GC)_3(AU)(GC)_3$, but the 2-fold symmetry of the helix about the middle (AU) prevents the unambiguous alignment of the connectivity-related set of resonances with the helix. Both terminal stem strand sequences are, in addition, nearly perfectly self-complementary so that 5S RNA strands which include either bases 1–10 or 110–120, but not both, are capable of dimerization. Dimers of both types have been examined and the NOE connectivities established. It is shown by using published ring current shift prediction rules that only one of the two possible alignments of resonances with the terminal helix is consistent with the chemical shifts of the resonances observed in all three species, the two dimers, and the native structure. Thus, the ambiguity of resonance assignments in the terminal helix is lifted.

In a model of the terminal helix structure which assumes that it is an A-type (11-fold) RNA double helix, there is a significant difference in the distances between the middle AU imino proton and the neighboring GC base pair imino protons. The time development of selective NOE effects (Dubs et al., 1979; Wagner & Wuthrich, 1979; Dobson et al., 1982) from the AU imino proton to its two neighboring GC imino protons should be strongly influenced by these differences in the interproton distances. The cross-relaxation rates of the AU imino proton to close protons were measured, and the interproton distances were derived. The measured distances cor-

† From the Department of Chemistry, Yale University, New Haven, Connecticut 06511. *Received November 17, 1983.* This research was supported by grants from the National Institutes of Health (AI-09167 and GM-32206). NMR spectroscopy was done at the Northeast Regional NMR Facility which is supported by the National Science Foundation (CHE-7916210). M.J.K. is a NATO/British Science and Engineering Research Council postdoctoral fellow.

[1] Abbreviations: NMR, nuclear magnetic resonance; Tris, tris(hydroxymethyl)aminomethane; NOE, nuclear Overhauser enhancement; RNA, ribonucleic acid; TEMED, *N,N,N',N'*-tetramethylethylenediamine; EDTA, disodium ethylenediaminetetraacetate; RNase, ribonuclease; SDS, sodium dodecyl sulfate.

0006-2960/84/0423-3559$01.50/0

respond well to those calculated for the terminal helix, assuming it is an A-type (11-fold) RNA helix, provided the resonances of the CG imino protons on both sides of the middle AU are assigned in the manner indicated by chemical shift criteria, confirming those assignments.

A biomolecular "reconstituted fragment" consisting of strands including bases 1–10 and bases 69–120 has also been examined. Species containing an isolated strand including the unbroken 79–97 sequence appear capable, upon "renaturation", of forming a procaryotic loop helix with a different structure to that in native fragment. Thus, (at least) two forms of the procaryotic loop helix can exist: (1) that found in isolated 5S RNA, or RNA fragment, and (2) that found in isolated continuous strands containing the procaryotic loop sequence after " renaturation" or after such strands have been incorporated into reconstituted fragment.

Materials and Methods

5S RNA. The 5S used for the work described here was rrnB 5S RNA unless explicitly stated otherwise. Details of the isolation of this rrnB 5S RNA following overproduction in the presence of chloramphenicol have been published (Kime & Moore, 1983a). This overproduced molecule has not been incorporated into ribosomes in the cell and in consequence is not fully mature (Feunteun et al., 1972). The differences from mature rrnB 5S RNA are (i) the 5′ end of the molecule is extended by up to four bases ($^{5'}$AAUU$^{3'}$) and (ii) the 3′ end of the molecule is extended by up to two bases ($^{5'}$CA$^{3'}$) (J. Normanly and H. F. Noller, personal communication).

The rrnB 5S is synthesized from one of seven ribosomal gene sets in *E. coli* (Kenerley et al., 1977; Kiss et al., 1977). rrnB 5S RNA differs from the canonical form of *E. coli* 5S RNA in having an adenine rather than a cytidine at position 12 (Brosius et al., 1981).

5S RNA Fragment. 5S RNA was treated with RNase A to generate fragment as described earlier (Kime & Moore, 1983a). RNA was dissolved in 0.1 M KCl, 5 mM $MgCl_2$, and 50 mM Tris–borate, pH 7.8, at a concentration of 20 A_{260nm}/mL. RNase A (Worthington) was added at concentrations from 1 to 10 μg/mL and digestion allowed to proceed at 0 °C for 45 min. The reaction was stopped by addition of SDS at 0.5% followed by phenol extraction. The ethanol precipitated product was purified by chromatography on Sephadex G-75 in 0.1 M NaCl, 5 mM $MgCl_2$, and 10 mM cacodylate buffer, pH 6.0 at 35 °C; 0.2 g/L of sodium azide was included in these buffers to prevent microbial contamination.

Oligonucleotide Separation. Preparative scale separation of oligonucleotide mixtures was done by chromatography on Sephadex G-75 in 8 M urea, 50 mM NaCl, 1 mM EDTA, and 10 mM cacodylate, pH 6.0 at 55 °C. The resolution achieved was sensitive both to temperature and to ionic conditions. Following pooling of the desired fractions, the samples were made 10 mM in Mg^{2+} and then dialyzed for 3–5 h against 0.1 M NaCl, 10 mM $MgCl_2$, and 10 mM cacodylate, pH 6.0, in the cold to remove urea. The RNA in the urea–free samples was then recovered by ethanol precipitation.

RNA Sequencing. The oligonucleotides studied in this work were characterized by sequencing using the method of Donis-Keller et al. (1977). Most of the sequences were determined by analysis of oligonucleotides labeled at the 5′ end with T4 polynucleotide kinase (Bethesda Research Laboratories).

Gel Electrophoresis. RNA and RNA/protein complexes were examined on "native" acrylamide gels. The gel composition was 10% acrylamide, 0.5% bisacrylamide, 0.08% TEMED, and 0.05% ammonium persulphate. The buffer used was 0.1 M KCl, 5 mM $MgCl_2$, and 50 mM Tris–borate, pH 7.8. Gels were run for 3 V/cm for 16 h at room temperature.

Oligonucleotides were examined on "denaturing" acrylamide/urea gels. The gel composition was 12% acrylamide, 8 M urea, 0.5% bis(acrylamide), 0.08% TEMED, and 0.05% ammonium persulfate. The buffer used was 89 mM Tris–borate and 2.5 mM EDTA, pH 8.3.

NMR Samples. RNA was dialyzed into 4 mM $MgCl_2$, 0.1 M KCl, and 5 mM cacodylate, pH 7.2 ("NMR buffer"). The fragment sample prepared for the time-dependent NOE experiments, however, was in the same buffer, but at pH 6.0. The material was subsequently dialyzed into NMR buffer containing 5% D_2O. Such samples were concentrated to a volume of ca. 0.5 mL by ultrafiltration (Amicon YM-5 membrane). Two microliters of 1 M aqueous dioxan was added to each sample as a chemical shift reference. The sample pH was determined by measurement of the pH of the ultrafiltrate.

Concentrations were estimated from absorbance at 260 nm by using 847 OD/mL as equivalent to a 1 mM solution of ribosomal 5S RNA (Osterberg et al., 1976) and assuming that the extinction coefficients of the strands are determined by the number of bases (with the hyperchromicity per base the same as that of the 5S RNA).

NMR Spectroscopy. This was performed by using the 45°-delay-45° pulse sequence described previously (Kime & Moore, 1983c). Data were collected at 303 K unless otherwise stated. Absolute intensity spectra (acquired by using a pulse cycle time of greater than 5 s to allow complete relexation of macromolecular protons between pulses) were recorded by using 32 K block sizes. NOE difference spectra were acquired in an interleaved fashion using 8 K block sizes. Presaturation pulse lengths of 300 ms were used, unless otherwise noted, in pulse cycle times of 0.5 s.

Time-dependent NOEs were acquired in a similar fashion to other NOE difference spectra but in 16 K block sizes and by using block averaging of as many data sets as were required to give adequate signal-to-noise difference spectra for the length of the presaturation pulse employed. A 1.5-s relaxation delay was inserted after each transient, making the pulse cycle time approximately $(1.75 + t)$ s where t was the length of the presaturation pulse. The time-dependent NOE data were analyzed by processing the difference spectra similarly and plotting them. The best "by-eye" base line for resonances of interest was drawn on the spectra, and the height of the resonances were measured. The NOE magnitude was expressed relative to the average intensity, in the control spectrum, of the resonance irradiated and its better resolved adjacent downfield resonance (both resonances were consistently found to be of almost equal intensity).

The data from selective irradiations for 0, 0.1, 0.15, 0.2, and 0.25 s are fitted to a straight line as an approximation to the initial time dependences of the NOEs. No allowance is made for the facts that the intensity data for short, nonzero, irradiation times are less accurately measured than those for longer irradiations and that intensity measurements for the resonance M are less accurate than those from protons closer to the saturated proton.

Results

Oligonucleotide Composition of 5S RNA Fragment. As was shown by Douthwaite et al. (1979), the oligonucleotide composition of 5S fragment can be displayed on urea/acrylamide gels. Figure 1a, lane 1, shows such an analysis of a fragment preparation made by digesting 5S RNA under standard conditions with RNase A at 1 μg/mL. Four com-

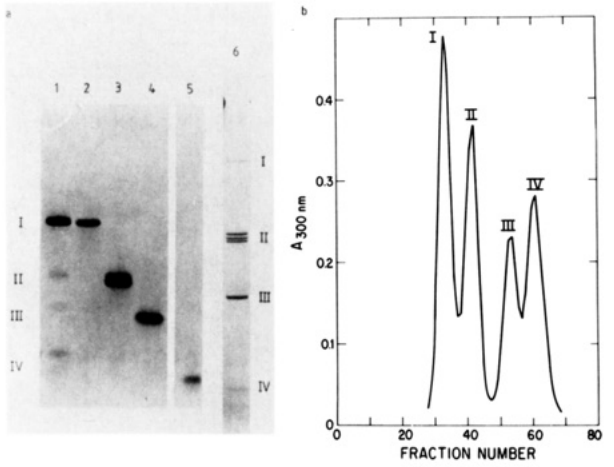

FIGURE 1: (a) Urea/acrylamide gel results with rrnB fragment and the component strands of fragment. Two experiments are shown. Lanes 1–5 were run on gels with 12% acrylamide, 8 M urea, 0.5% bisacrylamide, 0.08% TEMED, and 0.05% ammonium persulfate. The buffer used was 89 mM Tris–borate and 2.5 mM EDTA at pH 8.3. Runs were done at 3 V/cm for 16 h at ambient temperature, and buffer was recirculated to stabilize the pH. Lane 1, fragment prepared by digesting 5S RNA at 20 A_{260nm}/mL and 0 °C with 1 μg/mL ribonuclease A; lanes 2–5, the components of fragment isolated by chromatography on Sephadex G-75 in 8 M urea, 50 mM NaCl, 1 mM EDTA, and 10 mM cacodylate, pH 6.0 at 50 °C. Lane 2, strand I; lane 3, strand II; lane 4, strand III; lane 5, strand IV. Lane 6 comes from a long, high-resolution sequencing-type gel [36 cm long, 20% acrylamide, 0.67% *N,N'*-methylenebis(acrylamide), 7 M urea, 50 mM Tris–borate, 1 mM EDTA, and a gel buffer of 50 mM Tris–borate/1 mM EDTA at pH 8.3] which displays the composition of the fragment used for lane 1. These gels were visualized by staining with methylene blue. (b) Fragment prepared as in (a) was separated into its component oligonucleotides by chromatography on Sephadex G-75 in 8 M urea, 50 mM NaCl, 1 mM EDTA, and 10 mM cacodylate, pH 6.0 at 50 °C. The elution profile as measured by absorbance at 300 nm is shown.

ponents are seen. They are designated by numbers from high molecular weight (I) to low molecular weight (IV). The three smaller components should correspond to the oligonucleotides identified by Douthwaite et al. (1979) in denatured fragment preparations; II should be (approximately) bases 89–120 of the parent sequence, III should consist of bases 69–87, and IV should correspond to bases 1–11. The largest oligonucleotide, I was not identified by Douthwaite et al. (1979), who analyzed fragment prepared by more vigorous digestion, but it has a mobility appropriate for the complete sequence from 69 to 120. This result suggests that fragment can be prepared by RNase A digestion without cleavage necessarily occurring near bases 87–89. [This site at the end of the procaryotic loop was previously identified as a primary ribonuclease A cutting site (Douthwaite & Garrett, 1981)].

Figure 1b shows the result of chromatography of a fragment preparation on Sephadex G-75 in 8 M urea, 50 mM NaCl, 1 mM EDTA, and 10 mM cacodylate buffer, pH 6.0 at 50 °C. Four components are resolved. When these are examined on denaturing gels (Figure 1a, lanes 2–5), they are found to consist of the four components seen in lane 1, virtually pure. It was found that the yield of component I relative to components II and III can be controlled by adjusting the amount of RNase A used in the digestion. At 10 μg/mL RNase A, under standard conditions, the yield is about 10%. At 1.2–1.0 μg/mL the yield can approach 75%. Below 1 μg/mL the digestion begins to yield appreciable amounts of oligonucleotides larger than I, some which are visible in Figure 1a, lane 1, which makes isolation of pure I difficult.

Oligonucleotide Sequences. Figure 1a, lane 6, shows the result of electrophoresing 5S fragment on a 20% acrylamide/urea gel which is twice the length of the gels shown in lanes 1–5. The RNA components are visualized by methylene blue staining; band intensity is approximately proportional to the amount of RNA present in the band.

On high-resolution gels, strand I is predominantly a single-sized component. Sequencing done as described under Materials and Methods demonstrated that its 5′ end is base 69 of the parent sequence and its 3′ end is base 120. The strand II material isolated on Sephadex is a family of molecules which includes all possible species with 5′ ends of bases 88, 89, or 90 and with 3′ ends of bases 120, 121, or 122, bases C121 and A122 being the extensions beyond the 3′ end of the normal, mature 5S RNA. Strand III is about 90% a single species comprising bases 69–87 of the parent sequence. Strand IV is again a family of related molecules, like strand II. The largest member starts $^{5'}$UU and then continues with bases 1–10 of the parent molecule. Two shorter members lack one or both of the "extra" U's at the 5′ end, but these also end at base 10. Radiolabeling revealed traces of a 2–10 strand. The sequencing data are self-consistent except in one respect. The results with strand II imply the existence of three possible 3′-OH ends for RNase digested rrnB 5S near base 120. Thus, strand I should have been a family of three species differing in length. Only one was detected.

The sequencing results essentially confirm the analysis by Douthwaite et al. (1979) of fragment prepared from mature ribosomal 5S RNA (which differs from the rrnB-derived material studied here). It should be noted, however, that the RNase A, which cuts on the 3′ side of C11 in ribosomal 5S RNA [Douthwaite et al. (1979) and confirmed in this study], was found to consistently cleave the rrnB 5S material on the 3′ side of G10. This rrnB 5S cleavage does not follow the accepted specificity of RNase A which is to cut on the 3′ side of pyrimidine nucleotides. The difference between the cleavage positions in the two types of 5S RNA is probably a consequence of their sequence difference at position 12. The A12 of rrnB 5S may alter the conformation of the rrnB 5S RNA near positions 10–14 and render the G10–C11 linkage more accessible to RNase A than the G10–C11 linkage in the canonical 5S RNA which has a C at position 12. The results also show that most of the fractions which were studied by NMR spectroscopy (see below) are mixtures of oligonucleotides of closely related sequences and sizes, not pure species. Where references are made in this text to "strand II" or "strand IV" or any of the other strands, it should be understood that it is the whole family that is implied, not a single unique species.

Figure 2a shows the sequence of *E. coli* rrnB 5S RNA displayed in a slightly modified version of the Fox–Woese secondary structure (Garrett et al., 1981). The positions of the oligonucleotide strands in the sequence are indicated.

NMR Spectrum of Lightly RNase Digested Fragment. Figure 3a shows the absolute intensity spectrum at 296 K of a sample of fragment which is a mixture of mainly bimolecular fragment and some trimolecular fragment, produced by digestion of rrnB 5S RNA with 1 μg/mL RNase A under standard conditions. Figure 3b shows the same data after resolution enhancement. Preparations similar to this were used to prepare strand I. Figure 3c shows the resolution enhanced spectrum at 296 K of rrnB 5S RNA fragment produced by a similar digestion but by using 10 μg/mL RNase A. This sample was approximately 90% trimolecular fragment. Several differences are apparent. For example, resonance G is represented by a peak with an intensity (in absolute intensity spectra) which appears directly proportional to the amount

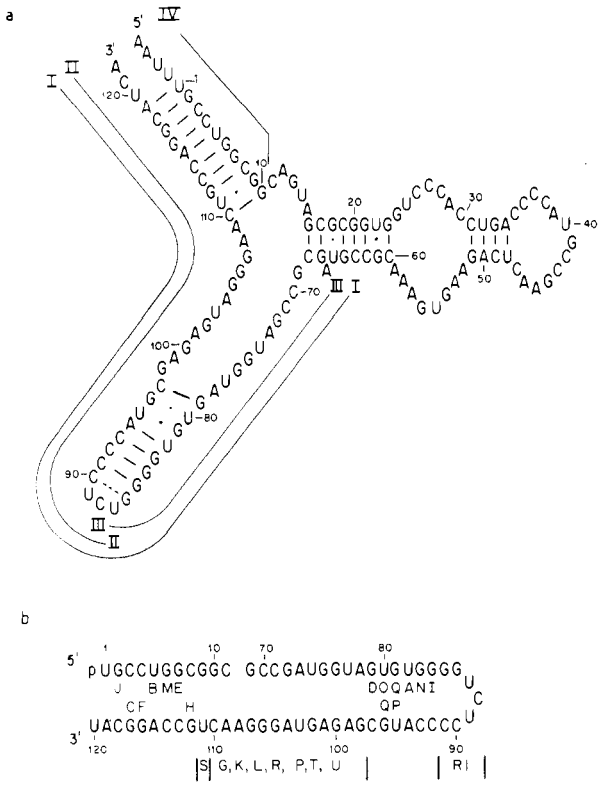

FIGURE 2: 5S RNA secondary structure. (a) *E. coli* 5S RNA is depicted in the three-stem secondary structure form proposed by Fox & Woese (1975). The version of that structure shown here is the one recently proposed by Garrett et al. (1981). This figure is redrawn with minor modifications from Figure 1 in Garrett et al. (1981). The oligonucleotide strands are indicated. (b) The assigned resonances are related to the fragment secondary structure. Firm assignments are indicated within the enclosed structure, and tentative assignments to regions of the molecule are marked below the structure.

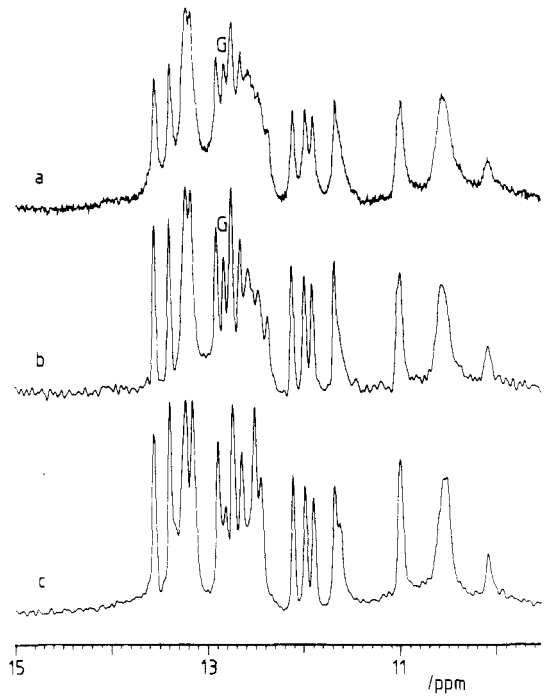

FIGURE 3: Downfield proton spectra of rrnB fragments recorded at 296 K. (a) An absolute intensity spectrum of an approximately 1 mM sample of mixed bimolecular and trimolecular fragment in 4 mM $MgCl_2$, 0.1 M KCl, and 5 mM cacodylate at pH 7.2. (b) The data of spectrum a after Lorentzian-to-Gaussian resolution enhancement. (c) A 2.5 mM sample of predominantly trimolecular fragment in 4 mM $MgCl_2$, 0.1 M KCl, and 5 mM cacodylate at pH 7.2.

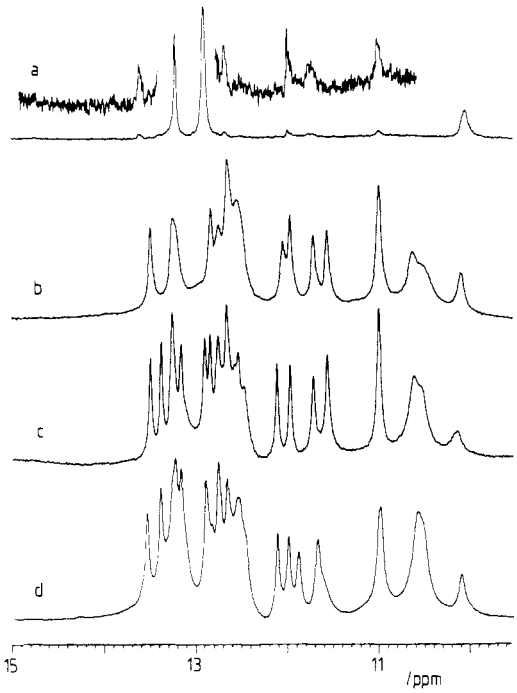

FIGURE 4: Absolute intensity downfield proton spectra recorded at 303 K. (Spectrum a) A 2.0 mM sample of strand IV in 4 mM $MgCl_2$, 0.1 M KCl, and 5 mM cacodylate at pH 7.2. (Spectrum b) A 1.2 mM sample of strand I in an identical buffer. (Spectrum c) A 0.7 mM reconstituted fragment sample in an identical buffer. (Spectrum d) A 2.5 mM sample of rrnB fragment in an identical buffer.

of bimolecular fragment present. There are also significant differences between bimolecular and trimolecular fragment spectra near 12.5 ppm.

NMR Spectrum of Strands and Reconstituted Fragment. Figure 4 shows absolute intensity spectra of (a), strand IV, (b), strand I (c), the reconstituted bimolecular complex made of strand I and IV (reconstituted fragment), and (d) the essentially trimolecular, unreconstituted, complex ("fragment"). In order to assist the reader in comparing the spectra of Figure 4, the same data are presented in resolution-enhanced form in Figure 5. The letters designating the fragment resonances (spectrum d) are taken from previous publications (Kime & Moore, 1983a). The designations given to the resonances of spectra a–c are at this stage to be considered as being based only on chemical shift comparisons with resonances in the fragment spectrum d.

Strand I. NOE difference spectra were obtained in which each of the resonances in the strand I spectrum was selectively irradiated. The results (not shown) indicate the existence of RNA double-helical structures of the forms $(X)(CG)_2$-(AU)(GU), (GU)(CG), and $(CG)_3(Y)$ where the resonances related are R1, I, N, A, $\overset{P}{Q}$ and $\overset{O}{Q}$, D and M, E, H, S, respectively. Inspection of the sequence of strand I suggests that the R1, I, N, A, $\overset{P}{Q}$ and the $\overset{O}{Q}$, D structures correspond to the procaryotic loop helix (I, N, A, $\overset{P}{Q}$ and $\overset{O}{Q}$, D) previously assigned in the fragment (Kime & Moore, 1983a,b), the intact 5S RNA, and L25 nucleoprotein complexes (Kime & Moore, 1983b) (bases 79–84 and 92–97). The helical structure with which resonances M, E, H, S may be associated is not obvious in the strand I molecule (see Figure 2a). An M, E, H, S-like connectivity, however, is observed as one part of the terminal helix in both the fragment and intact 5S RNA studies (Kime & Moore 1983a,b), but this set of connected resonances starts in these two molecules with four additional NOE-connected resonances, J, C, F, B. The terminal helix (bases 1–8 and 112–119) is clearly not present in its entirety in strand I: resonances B and F are certainly absent, and no B, F, C, J

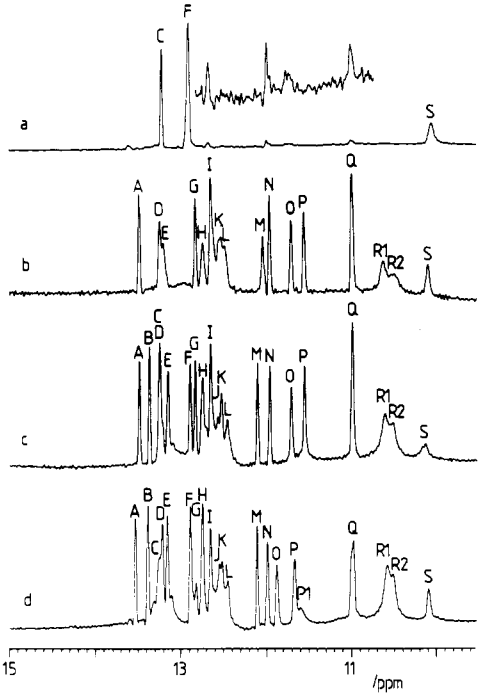

FIGURE 5: Data presented in Figure 4 after resolution enhancement.

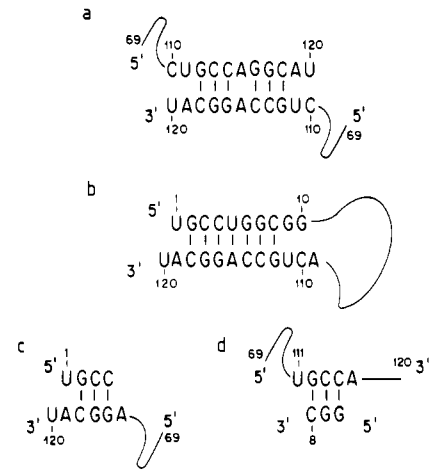

FIGURE 6: (a) Strand I dimer structure model. (b) The secondary structure of the terminal helix of 5S RNA and fragment. (c) The structure at the distal end of the 5S RNA terminal helix in common with the strand I dimer structure model. (d) The structure at the proximal end of the 5S RNA terminal helix in common with the strand I dimer structure model.

type connectivity may be detected. Moreover; the M, E, H resonances all appear to be broader and/or have small chemical shift changes relative to the comparable resonances in fragment spectra.

It is possible to construct a combined secondary and quaternary structure model for dimer formation by strand I (Figure 6a). This dimer model has a C2 axis of symmetry (for the species in which two identical strands combine and an effective C2 axis of symmetry for those complexes in which there are two strands combined which differ at the ends) which separates two identical short helices. Each short helix closely corresponds in sequence to either half of the terminal helix of both fragment and intact 5S RNA (Figure 6b–d). The detection of resonances M, E, H, S in the strand I spectrum indicates efficient strand I dimerization occurs under these conditions. This result is consistent with the detection of a species migrating slower than intact fragment in preparations of strand I on nondenaturing acrylamide gels, at much lower

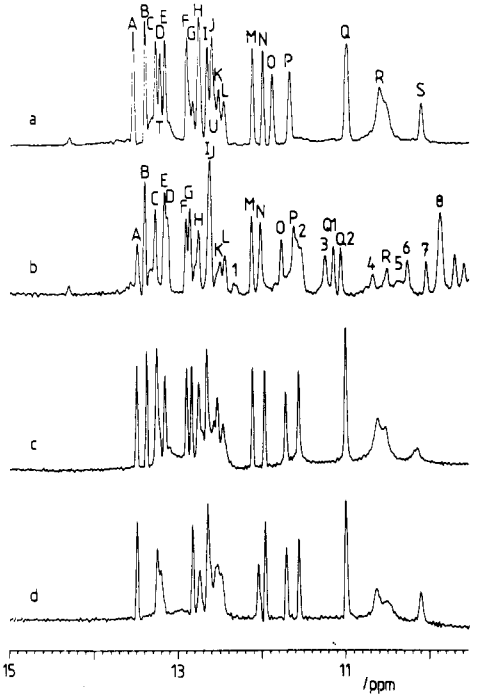

FIGURE 7: Comparison of some resolution-enhanced downfield proton spectra recorded at 303 K. (Spectrum a) 1 mM ribosomal fragment in 4 mM $MgCl_2$, 0.1 M KCl, and 5 mM cacodylate pH 7.2. (Spectrum b) Ribosomal fragment/L25 complex at a protein to RNA ratio of about 0.9:1 at about 1 mM in an identical buffer. (Spectrum c) 0.7 mM reconstituted fragment in an identical buffer. (Spectrum d) 1.2 mM strand I in an identical buffer.

concentrations (data not shown).

The strand I dimer M, E, H, S resonances are expected to be slightly different from their counterparts in fragment or intact 5S RNA because M is adjacent to an A–A opposition in the dimer rather than adjacent to an AU base pair as in the fragment or intact 5S. Also, there may be a related chemical exchange effect manifesting itself in the dimer M, E, H, S resonances. The line widths of well-resolved resonances in the strand I dimer appear to be slightly broader than comparable resonances of fragment spectra (rather than narrower as would be expected for strand I monomer). The dimer consists of about 100 bases whereas the fragment has bout 60 bases.

Examination of the chemical shifts of the procaryotic loop resonances in the strand I dimer spectrum reveals that resonances A and N are upfield shifted in the strand I dimer spectra relative to their positions in fragment spectra. Resonances O and P are considerably shifted upfield in the strand I dimer spectra relative to their positions in fragment spectra. Resonance D is slightly downfield shifted.

The chemical shift position of A in the strand I dimer spectra (and in the reconstituted fragment spectra; see later) exactly corresponds to the position this resonance assumes both in fragment and intact 5S RNA spectra upon binding ribosomal protein L25 (Figure 7). In the strand I dimer spectrum, O and P are close to the chemical shifts to which they move in the fragment or intact 5S RNA upon binding L25. Resonances Q1 and Q2, however, have chemical shifts close to those of fragment spectra. Thus, upon binding of L25, the imino protons giving rise to resonances A, O, and P in either fragment or intact 5S RNA experience an altered chemical environment very much like the one achieved in the absence of protein in the procaryotic loop helix of the strand I dimer.

Resonance R1 has not previously been connected by NOE to any resonance in either fragment or 5S RNA spectra. The

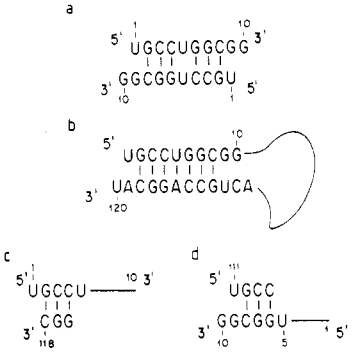

FIGURE 8: (a) Strand IV dimer structure model. (b) The secondary structure of the terminal helix. (c) The structure at the distal end of the 5S RNA terminal helix in common with the strand IV dimer structure model. (d) The structure at the proximal end of the 5S RNA terminal helix in common with the strand IV dimer structure model.

NOE connectivity to I observed in the strand I dimer must be established either as a consequence of a conformational change at the end of the procaryotic loop helix brought about by the renaturation process in the continuous RNA strand which is indicated by slightly "abnormal" chemical shifts of the procaryotic loop helix resonances or because the continuous RNA strand in its renatured form restricts solvent access so that imino proton exchange with solvent is slowed or both. The chemical shift of R1 suggests that the imino proton it represents is not involved in a stable base pair. It is likely that R1 corresponds to an imino proton which is detected spectroscopically because it is shielded from the solvent sufficiently to permit only slow proton exchange with the solvent, as has been suggested for an imino proton in a loop at the end of a helix formed by a one strand synthetic oligodeoxyribonucleotide (Haasnoot & Hilbers, 1983). This argument suggests that the imino proton of R1 is the N(1)H of G85.

Resonance G appears to exhibit a full stoichiometric intensity in the strand I dimer spectrum (and in the spectrum of reconstituted fragment; see below). It has not been connected by NOE to any other imino proton resonance; its identity is unknown.

Strand IV. This is the strand including the sequence that, in the intact 5S RNA, forms a perfect terminal double helix with the 3′ sequence of strand I. It is therefore base complementary to the terminal helix stretch of strand I and, by analogy with the behavior of the terminal helix sequence of strand I in solution, should be capable of dimerization. Such dimerization of strand IV would generate a C2 symmetrical dimer (with the proviso that some dimeric species will have slight asymmetry because of the differences at the ends of the strands) containing two short helices (see Figure 8a). Each short helix corresponds closely in sequence to either half of the terminal helix of both fragment and intact 5S RNA (Figure 8b–d). As previously mentioned, earlier work on both fragment and intact 5S RNA established that the terminal helix contained the base pair sequence $(CG)_3(AU)(CG)_3$ and this corresponded to the resonance NOE connectivity sequence H, E, M, B, F, C, J (Kime & Moore, 1983a). Figures 4a and 5a show the absolute intensity spectrum and the resolution enhanced spectrum, respectively, of strand IV. It is seen that the three resonances detected correspond, by chemical shift, quite closely to resonances C, F, and S of both fragment and intact 5S RNA. The short length of strand IV makes it highly unlikely that any helical structure could exist in the monomer because at least four bases would be needed to form a loop, and this would preclude the possibility of forming a helix long enough to be stable. On the face of it, it seems that strand I dimer has two identical helices (each of which has the M,

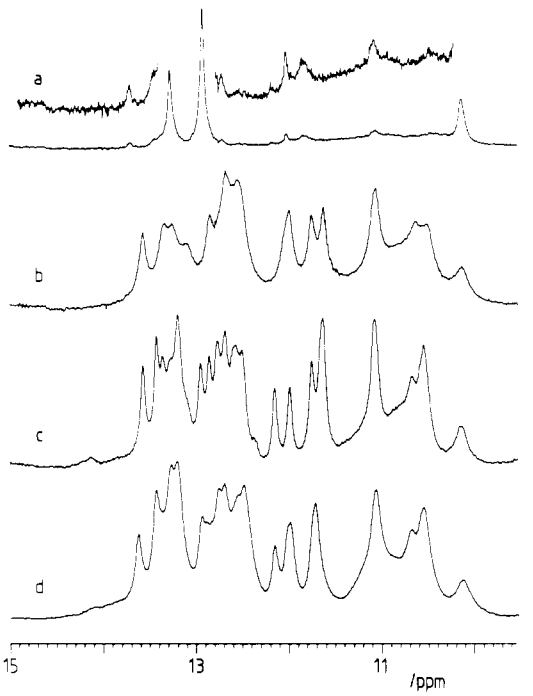

FIGURE 9: Absolute intensity downfield proton spectra recorded at 283 K on the samples described in Figure 4. (Spectrum a) Strand IV. (Spectrum b) Strand I. (Spectrum c) Reconstituted fragment. (Spectrum d) rrnB fragment.

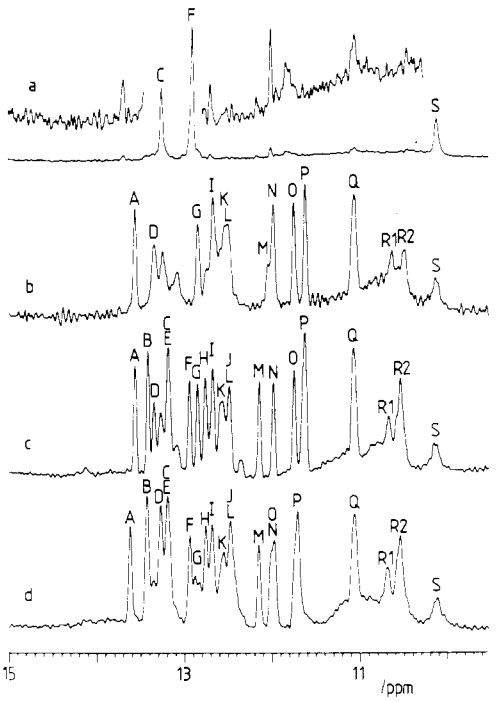

FIGURE 10: Data presented in Figure 9 after resolution enhancement.

E, H, S connectivity) and that strand IV has two identical helices (each of which has resonances C and F). To ensure that resonance J was not simply invisible because it was more exposed to solvent at the end of the helices in the short strand dimer (and so broadened by rapid exchange with the solvent), the strand IV spectrum was recorded at 283 K, and NOE experiments were performed.

Figure 9 shows the absolute intensity spectra of the same samples used to acquire the data of Figure 4 but recorded at 283 K. Figure 10 shows the same data after resolution enhancement. The letters designating the fragment resonances (spectrum d) are taken from previous publications (Kime &

Table I: Ring Current Shift Predictions for Base Pair Imino Proton Resonances of the Terminal Helix of *E. coli* 5S RNA and Comparison of the Predicted Chemical Shifts with Those Observed

	predicted ring current shifts (ppm)					predicted chemical shifts[a]					observed shifts[d]	
molecule	A[a]	A[b]	A'[b]	B[b]	A'[c]	A[a]	A[a]	A'[a]	B[b]	A'[c]	scheme I	scheme II
5S RNA/												
fragment												
U1 A119												
G2-C118	−0.78	−0.93	−1.01	−1.15	−1.2	−12.76	−12.57	−12.49	−12.35	−12.4	−12.59 (J)	−12.74 (H)
C3-G117	−0.26	−0.47	−0.51	−0.61	−0.45	−13.28	−13.03	−12.99	−12.89	−13.15	−13.27 (C)	−13.16 (E)
C4-G116	−0.52	−0.60	−0.66	−0.66	−0.8	−13.02	−12.90	−12.84	−12.84	−12.8	−12.89 (F)	−12.11 (M)
U5-A115	−0.65	−0.74	−0.83	−0.73	−1.2	−13.70	−13.61	−13.52	−13.62	−13.3	−13.39 (B)	−13.39 (B)
G6-C114	−1.07	−1.24	−1.36	−1.34	−1.7	−12.47	−12.26	−12.14	−12.16	−11.9	−12.11 (M)	−12.89 (F)
G7-C113	−0.26	−0.40	−0.44	−0.50	−0.45	−13.28	−13.10	−13.06	−13.00	−13.15	−13.16 (E)	−13.27 (C)
C8-G112	−0.56				−0.9	−12.98				−12.7	−12.74 (H)	−12.59 (J)
G9 U111												
strand I												
dimer												
U111 A119												
G112-C118	−0.78	−0.93	−1.01	−1.15	−1.2	−12.76	−12.57	−12.49	−12.35	−12.4	−12.74	
C113-G117	−0.26	−0.43	−0.48	−0.51	−0.45	−13.28	−13.07	−13.02	−12.99	−13.15	−13.21	
C114-G116	−1.10				−1.7	−12.44				−11.9	−12.04	
A115 A115												
strand IV												
dimer												
U1 G9												
G2-C8	−0.56				−0.9	−12.98				−12.7	−12.91	
C3-G7	−0.26	−0.32	−0.36	−0.32	−0.45	−13.28	−13.18	−13.14	−13.18	−13.15	−13.22	
C4-G6	−0.49				−0.8	−13.05				−12.8	−12.91	
U5 U5												

[a] Prediction method was from Robillard (1977). [b] Prediction method was from Arter & Schmidt (1976). [c] Prediction method was from Kearns (1976). [d] The observed chemical shift values for fragment spectra resonances are presented in both of the two assignment scheme alternatives permitted by the NOE evidence. These observed chemical shift values for the intact terminal helix were measured on a sample which was 1 mM ribosomal fragment in 0.1 M KCl, 4 mM $MgCl_2$, and 5 mM cacodylic acid, pH 7.2 at 303 K. The observed chemical shift values for the dimer spectra were taken from the data presented in Figures 3 and 4.

Moore, 1983a) and are directly related to the letters used for the comparable fragment resonances in spectra recorded at 303 K. Again the letters designating the resonances of spectra a–c are at this stage to be considered as letters of resonances in the fragment to which they may correspond on the basis of chemical shift comparisons.

There is no new resonance at 283 K. Resonances C and F were connected. Irradiation of S showed a connectivity to F, but the reverse connectivity was not detected. Resonance F at both 283 and 303 K has a downfield shoulder, and the intensity of the compound resonance (as judged by comparison of areas) appears about double that of either of the other two resonances, suggesting the spectrum includes two resonances at F and one at C.

Ring Current Shifts. Inspection of the data contained in Figures 6 and 8 did not immediately indicate why either of the dimer models should appear more like half of the intact terminal helix than the other. Furthermore, spectroscopic evidence for assignment of the dimer resonances to specific imino protons in the intact molecule terminal helix was not convincing. To resolve the ambiguity a model of the terminal helix was built, assuming that it was an A-form (11 base pair turn) helix. Examination of the model quite strongly favored the assignment which was consistent with 3'-side neighbors strongly influencing the base pair imino proton chemical shift. This was also a conclusion of the combined theoretical and empirical studies of ring current shift prediction used for assignment of imino protons in tRNA spectra [e.g., see Robillard (1977)]. Several of the published ring current shift prediction schemes were used to predict the chemical shifts of the terminal stem of fragment, the strand I dimer, and the strand IV dimer. These different prediction methods agree with each other with respect to the chemical shift order of the resonances in all three structures. Predicted values are compared with observed values in Table I.

There are two possible ways to assign resonances to the terminal stem on the basis of NOE results alone. Reading from the terminal to the proximal end one could suggest (1) J, C, F, B, M, E, H or (2) H, E, M, B, F, C, J. Comparison of predicted values with observed values (particularly those of the resonances from the base pairs on either side of the AU which gives rise to resonance B) reveals that assignment 2 is qualitatively incompatible with all the prediction schemes tested whereas assignment 1 is compatible. Thus, resonance J must correspond to the G2-C118 imino proton, and the rest of the terminal stem assignments follow. In addition, there is a good correspondence between predicted and experimental results for the resonances of the stem imino protons of the two dimers, lending further support for the assignments made for the 5S and fragment terminal stem helices. Thus, the correct ordering of the terminal stem resonances with respect to the sequence has been established.

Time-Dependent NOEs on Fragment. Examination of the A-form helical model of the terminal helix reveals that the imino protons of the CG base pair neighbors of the middle AU base pair differ in their distances from the AU imino proton. Presaturation of the AU imino proton resonance (labeled B in Figure 11a) with varying durations of the presaturation pulse (at constant decoupling power) allows examination of the relative contributions of the major centers of relaxation for the irradiated proton. In particular, studies of the initial relaxation of the saturated proton reveal dipolar relaxation rates by protons in the immediate vicinity of the irradiated proton. (At longer presaturation times other relaxation processes and relaxation by more distant centers become significant.) The cross-relaxation rates between close protons have the $r^{1/6}$ distance dependence of dipolar relaxation, and so time-dependent NOE data contain distance information. Known distances may be used to calibrate the distance dependence of the NOE, and so distance measurements may be

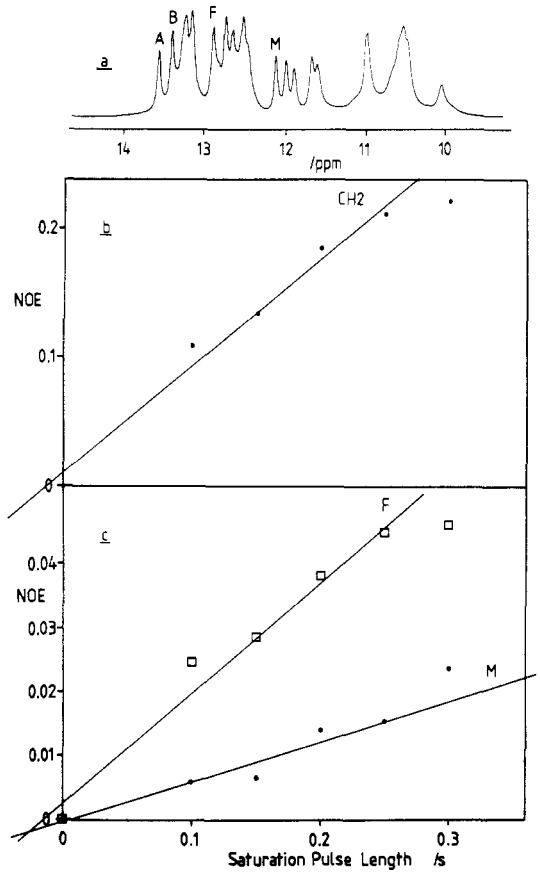

FIGURE 11: Time-dependent NOE data recorded at 300 K on 3.5 mM rrnB fragment in 4 mM $MgCl_2$, 0.1 M KCl, and 5 mM cacodylate at pH 6.0. (a) The off-resonance downfield proton spectrum. (b) The time development of the NOE to the A116 CH2 when the A116-U5 imino proton resonance is saturated. (c) The time development of the NOEs to resonances F and M when resonance B is selectively irradiated.

performed.

Here the imino proton of the middle AU base pair (assigned to resonance B) was irradiated, and then the NOEs to the neighboring CG base pair imino protons (resonances F and M) and the aromatic proton with a sharp resonance at 6.9 ppm (assumed to be the C2H of the middle AU) were studied as a function of the presaturation pulse length.

Figure 11b shows the data obtained on rrnB fragment at pH 6.0. This pH was chosen because imino proton exchange is slower than at higher pH values, and no other effects upon the structure are apparent. The rrnB fragment has a better resolved resonance B because resonance C is upfield shifted relative to the ribosomal fragment (the extensions on the 5′ and 3′ ends affect both C and J resonances in the rrnB fragment spectra) and the saturation of C would affect the apparent NOE to resonance F. In addition, fragment is more soluble at pH 6.0 than at pH 7.2. Resonance F has a significantly higher cross-relaxation rate than resonance M. Therefore, the resonance F proton is closer to the AU imino proton than the resonance M proton. The model of the terminal helix has the C4-G116 imino proton closer than the G6-C114 imino proton so resonance F is C4-G116 and resonance M is G6-C114. This confirms the alignment scheme arrived at by comparison of chemical shift predictions with observed spectra.

The assumption that the middle AU of the terminal helix is a Watson–Crick AU base pair with a U5 imino proton–A115 C2 proton distance of 2.9 Å permits an estimate of the distances between the middle AU imino proton and the protons giving resonances F and M. The BF distance is 3.8 Å, and the BM distance is 4.5 Å.

The interatomic distances were also calculated by using model A-RNA double helix coordinates (Arnott et al., 1972). The positions for the imino protons were calculated by assuming N–H bond lengths of 1 Å, and the interproton distances were then computed. The calculated BF distance is 3.46 Å, and the BM distance is 4.47 Å. The agreement of these calculated values with the NOE-derived distances is satisfactory.

Reconstitution of Fragment. One goal of this work was to produce fragment samples which are unbroken at bases 87–89 by reconstitution of strands I and IV. The strands and mixtures of strands were examined on nondenaturing acrylamide gels. It was found that reforming the fragment from its pieces was not trivial. After considerable trial and error, the following procedure was arrived at. Strands I and IV were mixed in 8 M urea, 50 mM NaCl, 1 mM EDTA, and 10 mM cacodylate, pH 6.0, to give a total RNA concentration of 20 A_{260nm}/mL, with strand IV present in slight molar excess over strand I. The mixture was heated at 90 °C for 3 min and then dialyzed against 0.1 M KCl, 10 mM $MgCl_2$, and 10 mM cacodylate, pH 6.0 at room temperature. After 6 h the RNA was recovered by ethanol precipitation and purified on G-75 just like normal, native fragment.

The I–IV complex prepared in this way behaved on Sephadex G-75 as native fragment. It binds ribosomal protein L25 on gels like native fragment and competes with intact 5S RNA for L25 with an efficiency which is qualitatively indistinguishable from native fragment (data not shown).

Reconstituted Fragment. Figure 5c shows a reconstituted fragment spectrum. The reconstitution is seen to have been successful in the sense that a terminal helix has been regenerated. Resonance B—which represents the AU imino proton (bases U5 and A105) in the terminal stem and which is necessarily absent in strand I or strand IV dimers—is present with stoichiometric intensity. The similarities between the reconstituted fragment spectrum and the fragment, strand I, and the strand IV spectra (see Figure 5) mean that it is easier to compare the spectra than to attempt to describe the reconstituted fragment spectrum in detail.

Comparison of the Reconstituted Fragment Spectrum with Spectra of Related Molecules. Resonances A, O, and P in the reconstituted fragment spectrum are like those of the strand I dimer spectrum, at the chemical shifts to which the corresponding resonances in fragment or intact 5S RNA move upon binding ribosomal protein L25 (see Figure 7). This indicates that, although the reconstituted material is normal in terms of electrophoretic mobility etc., the native structure has not been fully restored. Resonances D, O, and P in the reconstituted fragment spectrum also have the chemical shifts characteristic of strand I dimer (as opposed to the chemical shifts in either fragment or intact 5S RNA spectra). Resonance G is present in the reconstituted fragment spectrum at stoichiometric intensity. Resonances H and S in the reconstituted fragment spectrum appear uncharacteristically broad, but they do possess the same chemical shifts as related resonances in native fragment spectra. In contrast to the resonances M and E in the strand I dimer spectrum, the resonances M and E in the reconstituted fragment spectrum have the chemical shifts and line widths of the corresponding resonances in fragment spectra.

Low-Temperature Studies of the Fragments and Strands. (1) Strand I. Figure 9b shows the resolution-enhanced spectrum of strand I at 283 K. Selective NOE difference

spectra were obtained which established the I, N, A, $\frac{P}{Q}$ and the $\frac{O}{Q}$, D connectivities.

(*2*) *Strand IV.* The NOE difference results at 283 K have been mentioned earlier.

(*3*) *Reconstituted Fragment.* Figure 9c shows the resolution-enhanced spectrum of the reconstituted fragment at 283 K. Selective NOE difference spectra were obtained which established the I, N, A, $\frac{P}{Q}$, the D, $\frac{O}{Q}$, and the J, C, F, B, M, E, H, S connectivities. At low temperature a GU base pair can be demonstrated in fragment and the fragment/L25 complex, which is not seen at room temperature, involving resonances P and R2 (Kime & Moore, 1983a,b). The same P and R2 GU base pair was detected in the reconstituted fragment, at low temperature, but not in the strand I dimer or the strand IV dimer.

(*4*) *Other Strands.* Strands II and III have been briefly examined by NMR spectroscopy of the isolated strands at 303 K. The strand III spectrum is almost featureless. The strand II spectrum has an imino proton region which suggests the presence of discrete structure, but the resonances are relatively broad and have not been interpreted at this stage.

Discussion

The assignment of RNA imino proton resonances by the combined strategies of ring current shift prediction, fragmentation, and NOE connectivity has resolved several assignment difficulties previously reported (Kime & Moore, 1983a,b). Most important, the mirror ambiguity of earlier assignments to the terminal helix has been resolved. Resonance S, on the other hand, has not been firmly assigned by the evidence presented. The chemical shift indicates that it is an imino proton (exchanging slowly with the solvent) which is not involved in a base pair, like the proton which gives rise to resonance R1. It is concluded, from the NOE evidence cited here and elsewhere (Kime & Moore, 1983a,b), that resonance S in the intact 5S RNA/fragment spectra is the N(1)H of G9 or the N(3)H of U111. This is based on the observation of S to H NOEs and the assignment of H to the inside of the terminal stem to bases G8 and C112. In the strand I dimer spectrum resonance S must be the N(3)H of U111 since G9 is not in the sequence, and in the strand IV dimer resonance S could be either the N(3)H of U1, the N(1)H of G9, or the N(3)H of U5. The strand I dimer assignment of resonance S to the N(3) of U111 strongly suggests that in the intact 5S RNA/fragment spectra resonance S is likely to be the N(3)H of the same base and that it is probably the N(3)H of U1 in the strand IV dimer spectrum which occupies an analogous position in the structure.

Upon formation of the L25/fragment or the L25/intact 5S RNA complex, the chemical shift of resonance S is altered relative to the free RNA position (if indeed resonance S exists at all in the complex spectra). A minor effect on resonance H was also noted previously upon binding of protein (Kime & Moore, 1983b). The observation that resonance S is affected by L25 binding (as is resonance H, albeit only slightly) indicates that L25 binding effects are not exclusively confined to the procaryotic loop helix as earlier suggested (Kime & Moore, 1983b). The assignment of the sense of the F, C, J, B, M, E, H, S resonances indicates that the junction between the terminal helix and the procaryotic loop arm is also affected by L25 binding.

This assignment of S in the intact 5S RNA/fragment to U111 (or possibly G9) apparently excludes the possibility that the GU detected at low temperatures in fragment spectra (Kime & Moore, 1983a,b) giving rise to resonances P and R2 is G9-U111. By elimination, the low-temperature stable GU could be G102-U74 in the so-called helix V (bases 70–75 and 101–106) of universal 5S RNA secondary structure models, the only remaining possibility (De Wachter et al., 1982; Delihas & Andersen, 1982). It is surprising that the GU at base 9 and the GC at base 10 apparently do not exist in these molecules because they represent a natural continuation of the terminal stem helix. However, the absence of detectable NOEs from either J or H to possible wobble base pair GU resonances is consistent with the view that such a continuation does not exist. In view of the above conclusions that the junction between the terminal helix and the procaryotic loop arm is affected by L25 binding and that P, R2 is a GU of helix V, it appears paradoxical that the P and R2 (GU) is unaffected by L25 binding as previously noted (Kime & Moore, 1983b) because it suggests L25 affects the procaryotic loop helix and the junction between the terminal helix and the procaryotic loop arm, but the helix V region is unaffected.

Resonance G is present at stoichiometric intensity in the strand I dimer spectra and the reconstituted fragment spectra. G is also detected at almost stoichiometric intensity in the spectrum of a fragment sample containing a high proportion of strand I. No NOE connectivity to or from resonance G has been established.

Resonances K, L, and R2 are detected in the strand I dimer spectra, but they have not been related by NOE connectivity to any other imino protons. As the number of assignments increases it appears increasingly likely that all or most of the resonances G, K, L, and R2 represent imino proton intensity from helix V of the universal 5S RNA secondary structure models. Some, or all, of these resonances could be tertiary base pair imino proton resonances, but the physical evidence that 5S fragment behaves as a more-or-less rigid rod in solution (N. B. Leontis and P. B. Moore, unpublished results) does not favor this alternative.

The procaryotic loop helix assignments in the strand I form have been extended by a NOE connectivity to R1. R1 is probably a non base paired imino proton, the N(1)H of G85, which only slowly exchanges with the solvent because it is shielded from the solvent. More significant, however, is the observation that in the absence of protein the RNA which forms the procaryotic loop helix can adopt a stable helical form which differs from that observed in either intact 5S RNA or fragment. It appears that the renaturation stage (dialysis out of urea solution into high magnesium conditions in which native type structures would be stable) "selected" the form of helix which was to be adopted by strand I and by reconstituted fragment. This observation may be pertinent to the in vivo 5S RNA folding process. The $(AU)(GU)_2(GC)$ part of the procaryotic loop helix has resonances with chemical shifts which differ from those of the corresponding imino proton resonances in both the isolated fragment and 5S RNA.

Ring current shift predictions were resorted to in this work not as a primary assignment tool but to distinguish between two distinctly different assignment schemes in the terminal stem, both of which were acceptable by NOE connectivity criteria. As should be obvious some assumptions were implicitly made when the two assignment schemes were tested by the ring current shift prediction schemes. In addition to the assumptions which were associated with each of the particular ring current shift schemes used, we assume where necessary that the (unpaired) nearest neighbors on both the 3′ and 5′ sides of base paired helices have the same effect on the terminal, base paired imino proton chemical shifts that they would exert if they were part of a longer helix. As the main ring current shift effect is caused by aromatic base

position which is determined to a significant extent by stacking considerations, not hydrogen bonding per se, this assumption does not appear unreasonable. Comparison of predicted data with experimental data for resonances which would be affected by this assumption encourages us that this assumption is valid for the system studied. [Examination of the predicted chemical shift values and the comparison of such data with experimental data show that the correlation is best for the values predicted for an A′-form RNA helix by Kearns (1976).]

In view of the availability of the NOE connectivity method of assignment of imino protons in nucleic acids, it would be wrong to advocate a return to the use of ring current shift prediction methods for assignments, but in view of the possibility of errors or ambiguities in the interpretation of NOE data, it appears prudent to check nucleic acid secondary structures proposed on the basis of NOE experiments/sequence studies by examining the compatability of the chemical shifts observed with those which would be predicted for that secondary structure and helix type. The ring current shift prediction method may be more applicable to other nucleic acids than it is to tRNA, for which it was originally developed, because tRNA is unusual in having many modified bases, in having lots of tertiary interactions, and in being particularly compact.

Likewise, the assignment strategy of nucleolytic fragment study by NOE connectivity may have a wider applicability in nucleic acid and nucleoprotein NMR spectroscopy than would be apparent on the basis of tRNA experience. Again this may reflect the particularly compact, globular, nature of tRNAs that could result in structural change effects being transmitted cooperatively throughout the intact molecule. Smaller derivatives of the molecules would not be subject to such influences, and therefore, comparison of their spectra with those of their parent molecules would be of dubious value for assignment.

Acknowledgments

This work was made possible by the kind gift of *E. coli* strain HB101/pKK5-1 from Drs. J. Brosius and H. Noller. We thank Joseph Schoeniger for helpful discussions. Betty Rennie and Grace Sun provided able technical assistance, and Susan Vrba assisted in the preparation of the manuscript. We thank the reviewer at whose suggestion the time-dependent NOE measurements were performed and added to the text.

References

Arnott, S., Hukins, D. W. L., & Dover, S. D. (1972) *Biochem. Biophys. Res. Commun. 48*, 1392–1399.

Arter, D. B., & Schmidt, P. G. (1976) *Nucleic Acids Res 3*, 1437–1447.

Boyle, J., Robillard, G. T., & Kim, S.-H. (1980) *J. Mol. Biol. 139*, 601–625.

Brosius, J., Dull, T. J., Sleeter, D. D., & Noller, H. F. (1981) *J. Mol. Biol. 148*, 107–127.

Delihas, N., & Andersen, J. (1982) *Nucleic Acids Res. 10*, 7323–7344.

De Wachter, R., Chen, M.-W., & Vandenberghe, A. (1982) *Biochimie 64*, 311–329.

Dobson, C. M., Olejniczak, E. T., Poulsen, F. M., & Ratcliffe, R. G. (1982) *J. Magn. Reson. 48*, 97–110.

Donis-Keller, H., Maxam, A. M., & Gilbert, W. (1977) *Nucleic Acids Res. 4*, 2527–2538.

Douthwaite, S., & Garrett, R. A. (1981) *Biochemistry 20*, 7301–7307.

Douthwaite, S., Garrett, R. A., Wagner, R., & Feunteun, J. (1979) *Nucleic Acids Res. 6*, 2453–2470.

Dubs, A., Wagner, G., & Wuthrich, K. (1979) *Biochim. Biophys. Acta 577*, 177–194.

Feunteun, J., Jordan, B. R., & Monier, R. (1972) *J. Mol. Biol. 70*, 465–474.

Fox, G. E., & Woese, C. R. (1975) *Nature (London) 256*, 505–506.

Garrett, R. A., Douthwaite, S., & Noller, H. F. (1981) *Trends Biochem. Sci. (Pers. Ed.) 6*, 137–139.

Haasnoot, C. A. G., & Hilbers, C. W. (1983) *Biopolymers 22*, 1259–1266.

Hare, D. R., & Reid, B. R. (1982) *Biochemistry 21*, 5129–5135.

Heerschap, A., Haasnoot, C. A. G., & Hilbers, C. W. (1983) *Nucleic Acids Res. 11*, 4501–4520.

Hurd, R. E., & Reid, B. R. (1979) *Biochemistry 18*, 4005–4011.

Johnston, P. D., & Redfield, A. G. (1981) *Biochemistry 20*, 1147–1156.

Kearns, D. R. (1976) *Prog. Nucleic Acid Res. Mol. Biol. 18*, 91–149.

Kenerley, M. E., Morgan, E. A., Post, L., Lindahl, L., & Nomura, M. (1977) *J. Bacteriol. 132*, 931–949.

Kime, M. J., & Moore, P. B. (1983a) *Biochemistry 22*, 2615–2622.

Kime, M. J., & Moore, P. B. (1983b) *Biochemistry 22*, 2622/2629.

Kime, M. J., & Moore, P. B. (1983c) *FEBS Lett. 153*, 199–203.

Kiss, A., Sain, B., & Venetianer, P. (1977) *FEBS Lett. 79*, 77–79.

Lightfoot, D. R., Wong, K. L., Kearns, D. R., Reid, B. R., & Shulman, R. G. (1973) *J. Mol. Biol. 78*, 71–89.

Osterberg, R., Sjoberg, B., & Garrett, R. A. (1976) *Eur. J. Biochem. 68*, 481–487.

Reid, B. R., McCollum, L., Ribeiro, N. S., Abbate, J., & Hurd, R. E. (1979) *Biochemistry 18*, 3996–4005.

Robillard, G. T. (1977) in *NMR in Biology* (Dwek, R. A., Campbell, I. D., Richards, R. E., & Williams, R. J. P., Eds.) pp 201–230, Academic Press, New York.

Roy, S., & Redfield, A. G. (1983) *Biochemistry 22*, 1386–1390.

Shulman, R. G., Hilbers, C. W., Kearns, D. R., Reid, B. R., & Wong, Y. P. (1973) *J. Mol. Biol. 78*, 57–69.

Wagner, G., & Wuthrich, K. (1979) *J. Magn. Reson. 33*, 675–680.